Published in final edited form as:
Magn Reson Med. 2012 August ; 68(2): 595–599. doi:10.1002/mrm.23262.

Theranostic effect of serial manganese-enhanced magnetic resonance imaging of human embryonic stem cell derived teratoma

Jaehoon Chung, MD[1], **Rajesh Dash, MD, PhD**[1], **Kehkooi Kee, PhD**[2], **Joëlle K. Barral, PhD**[3], **Hisanori Kosuge, MD, PhD**[1], **Robert C. Robbins, MD**[4], **Dwight Nishimura, PhD**[3], **Renee A. Reijo-Pera, PhD**[2], and **Phillip C. Yang, MD**[1]

[1]Department of Medicine, Stanford University, Stanford, CA, 94305

[2]Institute for Stem Cell Biology and Regenerative Medicine, Stanford University, Stanford, CA, 94305

[3]Department of Electrical Engineering, Stanford University, Stanford, CA, 94305

[4]Department of Cardiothoracic Surgery, Stanford University, Stanford, CA, 94305

Abstract

Although hESCs hold therapeutic potential, teratoma formation has deterred clinical translation. Manganese (Mn^{2+}) enters metabolically active cells through voltage-gated calcium channels and, subsequently, induces T_1 shortening. We hypothesized that serial MEMRI would have theranostic effect to assess hESC survival, teratoma formation, and hESC-derived teratoma reduction through intracellular accumulation of Mn^{2+}. Firefly luciferase transduced hESCs (hESC-Lucs) were transplanted into SCID mouse hindlimbs to form teratoma. The chemotherapy group was injected with $MnCl_2$ IP three times a week. The control group was given $MnCl_2$ only prior to MEMRI. Longitudinal evaluation by MEMRI and bioluminescence imaging (BLI) was performed. The chemotherapy group showed significant reduction in the teratoma volume and luciferase activity at weeks 6 and 8. Histology revealed increased proportion of dead cells and caspase 3 positive cells in the chemotherapy group. Systemic administration of $MnCl_2$ enabled simultaneous monitoring and elimination of hESC-derived teratoma cells by higher intracellular accumulation of Mn^{2+}.

Keywords

manganese enhanced MRI; embryonic stem cell derived teratoma

Introduction

Human embryonic stem cells (hESCs) are pluripotent, holding the potential to differentiate into mature adult cells(1). Several animal studies have reported that the hESCs significantly restore damaged organs(2–4). However, cellular engraftment is complicated by teratoma formation. Therefore, an *in vivo* imaging system to monitor stem cell survival while also detecting and treating teratoma without molecular manipulation of the stem cells has been developed in the current study.

Corresponding author: Phillip C. Yang[1], 300 Pasteur drive, H-2157, Stanford, CA 94305. Tel: 650-498-8008, Fax: 650-725-1599, pyang@cvmed.stanford.edu.

Manganese-enhanced MRI (MEMRI) employs unique property of manganese (Mn^{2+}), which enters only the metabolically active cells through voltage-gated calcium channels. Consequently, intracellular Mn^{2+} can induce T_1-shortening effect generating positive contrast in viable cells(5–7). Even though Mn^{2+} has been recognized as the first MRI contrast agent, known toxicity has hindered widespread use. Recently, sensitive *in vivo* detection of various cancers using MEMRI has been reported(8,9). This study represents the first feasibility study to assess the theranostic potential of MEMRI by *in vivo* longitudinal evaluation and therapy of hESC-derived teratoma cells.

Methods

Optimization of therapeutic dosage of $MnCl_2$

All the following animal protocols were approved by the administrative panel on laboratory animal care at Stanford University. The therapeutic dosage of $MnCl_2$ was optimized by administering tolerable maximal dosage of $MnCl_2$ in severe combined immunodeficient (SCID) mice.

Culture of undifferentiated hESC

The H9-line of hESCs (Wicell, Madison, WI) was trandscuded with firefly luciferase (hESC-Lucs) and maintained in an undifferentiated and pluripotent state by culturing on irradiated mEF feeder layer using the hESC culture medium(10).

hESC-derived teratoma formation and $MnCl_2$ chemotherapy

Under general anesthesia with 1% isoflurane at 1L/min oxygen, 1×10^6 of hESC-Luc were directly injected into SCID mouse hindlimbs by an insulin syringe (n=12). These mice were divided into two groups: chemotherapy and control groups. The chemotherapy group (n=6) was injected with 500 μl of 5 mM $MnCl_2$ intraperitoneally (IP) three days a week. The control group (n=6) was given 250 μl of 5 mM $MnCl_2$ IP only prior to image acquisition.

Serial in vivo MEMRI and BLI

Longitudinal *in vivo* evaluation by MEMRI and bioluminescence imaging (BLI) was performed on post-transplant weeks 2, 4, 6 and 8. For MEMRI, all the mice were injected with 250 μl of 5 mM $MnCl_2$ IP 15 minutes prior to imaging(7). Under general anesthesia by 1% isoflurane at 1L/min oxygen, each mouse was placed on top of a customized small animal surface coil in a prone position. Both hindlimbs were scanned using Signa 3.0 T Excite HD scanner (GE Healthcare system, Milwaukee, WI) with spin echo inversion recovery (SE IR) sequence: TR 600 ms, TE 5 ms, TI 120ms, NEX 1, FOV 3, slice thickness 0.8 mm, space 0 mm and matrix 128×128. MEMRI data were analyzed for contrast-to-noise-ratio (CNR) and 3D volume using image J (NIH, Bethesda, MD). CNR was calculated as follows: $CNR = (SI_{teratoma} - SI_{muscle}) / SD$ of the image noise. Under general anesthesia, concurrent BLI was performed using the charged-coupled device camera (IVIS spectrum, Caliper, Mt. view, CA) following IP injection of D-luciferin at 375mg/kg body weight. Bioluminescence images were acquired for 30 minutes at a 3 min interval and quantified in units of photons $\cdot$ $second^{-1}$ $\cdot$ $centimeter^{2-1}$ $\cdot$ $steridian^{-1}$ using Living image 2.5 (Caliper, Mt. view, CA)(11).

Histological analysis

At post-transplantation weeks 6 and 8, 3 mice in each group were sacrificed for histology. All the histological data were assessed by a veterinary pathologist, who was blinded to the study. Teratoma was processed for a paraffin block followed by H&E staining of 5 μm slice.

For caspase 3 detection, immunohistochemistry procedure was performed according to the manufacturer's manual (Vector laboratories Inc, Burlingame, CA).

Statistical analysis

Descriptive statistics include mean and standard deviation. Comparison between two groups was performed using student's *t*-test. Comparison among multiple groups was conducted using ANOVA with Post Hoc test. All data analyses were done by SPSS 16.0 (SPSS Inc, Chicago, IL). Significance was assumed when $p < 0.05$.

Results

Optimization of $MnCl_2$ administration

The chemotherapy protocol was optimized at 500 μl of 5 mM IP three times a week. All SCID mice tolerated the chemotherapy protocol for 8 weeks. But all the mice in the chemotherapy group developed feet swelling.

In vivo MEMRI and BLI of Cell Survival and Teratoma formation

CNR of the hESCs was compared with concurrent luciferase activity (Fig. 1A). With the hESC proliferation and subsequent teratoma formation, CNR and luciferase activity increased accordingly at each time point (Fig. 1B). These mice did not receive multiple doses of Mn^{2+} (chemotherapy group) but only prior to undergoing MEMRI (control group). Significant correlation was revealed between CNR and luciferase activity by Pearson correlation ($p<0.01$). Significant increase in CNR was noted at 6 weeks post-transplantation, corresponding with teratoma formation on the H & E staining (Fig. 1C).

In vivo MEMRI and BLI of Teratoma Reduction

The chemotherapy group showed significant reduction in the volume of teratoma compared to the control group (9.4±4.2 vs. 16.8±1 at week 6 and 64±49 vs. 123±70 at week 8, $p<0.05$, Fig. 2A). CNR was comparable between the chemotherapy and control groups throughout the 8 week period. At weeks 4 and 6, a trend towards higher CNR was demonstrated in the chemotherapy group. However, at week 8, CNR demonstrated a higher trend in the control group ($p>0.05$, Fig. 2B). BLI demonstrated a significantly decreased luciferase activity in the chemotherapy group compared to the control group at weeks 6 and 8 ($p<0.05$, Fig. 2C).

Histological analysis

H&E staining of teratoma in both groups revealed hESCs-derived mature teratoma at post-transplantation period, week 6. Development of three germ layers, consistent with teratoma formation, was similar between the two groups, suggesting Mn^{2+} does not affect the pluripotent property of hESCs (Fig. 3A). The chemotherapy group showed increased proportion of dead cells within the teratoma compared with the control group (Fig. 3B). Finally, immunohistochemistry demonstrated positivity for caspase-3 only at week 8 in the chemotherapy group, indicating apoptotic cell death while the control group did not show any caspase-3 signal (Fig. 3C).

Discussion

Even though several animal studies have demonstrated the enormous potential of hESCs to restore damaged organs, the formation of teratoma has been a major obstacle to clinical implementation of hESCs(12). To address this critical issue, we previously demonstrated sensitive and reliable *in vivo* detection of hESC-induced teratoma by MEMRI(7).

Interestingly, Mn^{2+} was reported as the first MRI contrast agent, which increased *R1* in the liver, kidney and heart(13). Since Mn^{2+} is a competitive inhibitor of calcium channel, it blocks calcium influx through the voltage-gated calcium channel in the heart and the brain, possibly compromising cardiac and neurologic function(14). Although little is known about Mn^{2+} interaction within the hESCs, it is bound to intracellular or nuclear calcium binding proteins and mostly taken up by mitochondria(15,16). The intracellular accumulation of Mn^{2+} by viable hESCs induces T1 shortening effect, generating positive MRI signal(6). Thus, MEMRI localizes viable hESCs, allowing accurate in vivo evaluation of the anatomical and biological properties following cell transplantation. However, cellular toxicity of Mn^{2+} has been known to cause cardiac toxicity by acute exposure and Parkinson-like symptoms following chronic exposure. Our data also showed higher concentration of Mn^{2+} caused extensive mineralization of myocardium, resultant fibrosis, and death in SCID mice. The increased Mn^{2+} uptake by the hESC-derived teratoma cells may be due to their enhanced metabolism and immature voltage-gated calcium channels, resulting in excessive intracellular accumulation and, subsequent, cell death(17–20). Future studies are planned to test this hypothesis by comparing the differential uptake of Mn^{2+} and the toxicity between the undifferentiated embryonic stem cells and embryonic stem cell derived cardiac cells.

Longitudinal assessment of the bio-kinetics of hESC-derived teratoma has demonstrated that Mn^{2+} could eliminate a substantial portion of the teratoma burden. Significant reduction in the 3-D volume and luciferase activity of the teratoma are generated at weeks 6 and 8 following serial systemic Mn^{2+} administration. This finding suggests that the cytotoxic effects could be reached by week 6. This finding is also corroborated with positive caspase 3 expression in the chemotherapy group only at week 8 and not week 6 in either group. Our laboratory has reported significant annexin expression by hESCs when cells are labeled with higher dose of manganese(7). In addition, several studies have shown manganese chloride induced apoptosis and cell death in various cell types(20–23). Thus, this study demonstrates that the increased intracellular accumulation of Mn^{2+} within the teratoma cells induces apoptosis and, subsequent, cell death.

The limitations of our study include the nonselective manganese uptake. Although the increased cellular metabolism and the immature calcium channels of the differentiating hESCs may underlie the mechanism for the MEMRI-mediated theranostic approach, a targeted approach will be desirable to avoid systemic toxicity(24). A novel method employing antibodies specific to the teratoma cells to deliver the Mn^{2+} nanoparticles is currently underway(25). Furthermore, complete eradication of the teratoma is not achieved. Differential uptake of manganese depending on the specific cell types within the teratoma may account for this finding(19,20). In addition, we do not compare the therapeutic efficacy of MEMRI with cisplatin based regimen. However, to the best of our knowledge, no report is available on the chemotherapeutic option against hESC-derived teratoma. Finally, we do not establish a correlation between the MEMRI signal and the histology of the early, proliferative stage of hESC growth. Comparison between MEMRI and traditional MRI methods at the early proliferative stage was also not performed.

In conclusion, this study demonstrates the feasibility of the theranostic capability of MEMRI to track the viable transplanted teratoma cells and attenuate the growth of the hypermetabolic teratoma cells.

Acknowledgments

The study was supported by the NIH R01 and CIRM training grant.

References

1. Boheler KR, Czyz J, Tweedie D, Yang HT, Anisimov SV, Wobus AM. Differentiation of pluripotent embryonic stem cells into cardiomyocytes. Circ Res. 2002; 91(3):189–201. [PubMed: 12169644]
2. Arai T, Kofidis T, Bulte JW, de Bruin J, Venook RD, Berry GJ, McConnell MV, Quertermous T, Robbins RC, Yang PC. Dual in vivo magnetic resonance evaluation of magnetically labeled mouse embryonic stem cells and cardiac function at 1.5 t. Magn Reson Med. 2006; 55(1):203–209. [PubMed: 16315206]
3. Singla DK, Lyons GE, Kamp TJ. Transplanted embryonic stem cells following mouse myocardial infarction inhibit apoptosis and cardiac remodeling. Am J Physiol Heart Circ Physiol. 2007; 293(2):H1308–H1314. [PubMed: 17416601]
4. Wong SS, Bernstein HS. Cardiac regeneration using human embryonic stem cells: producing cells for future therapy. Regen Med. 2010; 5(5):763–775. [PubMed: 20868331]
5. Aoki I, Takahashi Y, Chuang KH, Silva AC, Igarashi T, Tanaka C, Childs RW, Koretsky AP. Cell labeling for magnetic resonance imaging with the T1 agent manganese chloride. NMR Biomed. 2006; 19(1):50–59. [PubMed: 16411253]
6. Kang YS, Gore JC. Studies of tissue NMR relaxation enhancement by manganese. Dose and time dependences. Invest Radiol. 1984; 19(5):399–407. [PubMed: 6511248]
7. Yamada M, Gurney PT, Chung J, Kundu P, Drukker M, Smith AK, Weissman IL, Nishimura D, Robbins RC, Yang PC. Manganese-guided cellular MRI of human embryonic stem cell and human bone marrow stromal cell viability. Magn Reson Med. 2009; 62(4):1047–1054. [PubMed: 19526508]
8. Hasegawa S, Koshikawa-Yano M, Saito S, Morokoshi Y, Furukawa T, Aoki I, Saga T. Molecular imaging of mesothelioma by detection of manganese-superoxide dismutase activity using manganese-enhanced magnetic resonance imaging. Int J Cancer. 2010 May 1; 128(9):2138–2146. [PubMed: 20617513]
9. Seshadri M, Hoy A. Manganese-enhanced MRI of salivary glands and head and neck tumors in living subjects. Magnetic resonance in medicine : official journal of the Society of Magnetic Resonance in Medicine / Society of Magnetic Resonance in Medicine. 2010; 64(3):902–906. [PubMed: 20806380]
10. Reubinoff BE, Pera MF, Fong CY, Trounson A, Bongso A. Embryonic stem cell lines from human blastocysts: somatic differentiation in vitro. Nat Biotechnol. 2000; 18(4):399–404. [PubMed: 10748519]
11. Wu JC, Chen IY, Sundaresan G, Min JJ, De A, Qiao JH, Fishbein MC, Gambhir SS. Molecular imaging of cardiac cell transplantation in living animals using optical bioluminescence and positron emission tomography. Circulation. 2003; 108(11):1302–1305. [PubMed: 12963637]
12. Nussbaum J, Minami E, Laflamme MA, Virag JA, Ware CB, Masino A, Muskheli V, Pabon L, Reinecke H, Murry CE. Transplantation of undifferentiated murine embryonic stem cells in the heart: teratoma formation and immune response. FASEB J. 2007; 21(7):1345–1357. [PubMed: 17284483]
13. Mendonca-Dias MH, Gaggelli E, Lauterbur PC. Paramagnetic contrast agents in nuclear magnetic resonance medical imaging. Semin Nucl Med. 1983; 13(4):364–376. [PubMed: 6359418]
14. Wolf GL, Baum L. Cardiovascular toxicity and tissue proton T1 response to manganese injection in the dog and rabbit. AJR Am J Roentgenol. 1983; 141(1):193–197. [PubMed: 6305179]
15. Maynard LS, Cotzias GC. The partition of manganese among organs and intracellular organelles of the rat. J Biol Chem. 1955; 214(1):489–495. [PubMed: 14367406]
16. Hunter DR, Komai H, Haworth RA, Jackson MD, Berkoff HA. Comparison of Ca2+, Sr2+, and Mn2+ fluxes in mitochondria of the perfused rat heart. Circ Res. 1980; 47(5):721–727. [PubMed: 6774832]
17. Lewis BB, Wester MR, Miller LE, Nagarkar MD, Johnson MB, Saha MS. Cloning and characterization of voltage-gated calcium channel alpha1 subunits in Xenopus laevis during development. Dev Dyn. 2009; 238(11):2891–2902. [PubMed: 19795515]

18. An RH, Davies MP, Doevendans PA, Kubalak SW, Bangalore R, Chien KR, Kass RS. Developmental changes in beta-adrenergic modulation of L-type Ca2+ channels in embryonic mouse heart. Circ Res. 1996; 78(3):371–378. [PubMed: 8593695]

19. Choi JY, Lee SH, Na HB, An K, Hyeon T, Seo TS. In vitro cytotoxicity screening of water-dispersible metal oxide nanoparticles in human cell lines. Bioprocess Biosyst Eng. 2010; 33(1): 21–30. [PubMed: 19636592]

20. Thongphasuk J, Oberley LW, Oberley TD. Induction of superoxide dismutase and cytotoxicity by manganese in human breast cancer cells. Arch Biochem Biophys. 1999; 365(2):317–327. [PubMed: 10328827]

21. Tamm C, Sabri F, Ceccatelli S. Mitochondrial-mediated apoptosis in neural stem cells exposed to manganese. Toxicol Sci. 2008; 101(2):310–320. [PubMed: 17977900]

22. Park EJ, Park K. Induction of oxidative stress and inflammatory cytokines by manganese chloride in cultured T98G cells, human brain glioblastoma cell line. Toxicol In Vitro. 2010; 24(2):472–479. [PubMed: 19815061]

23. Li Y, Sun L, Cai T, Zhang Y, Lv S, Wang Y, Ye L. alpha-Synuclein overexpression during manganese-induced apoptosis in SH-SY5Y neuroblastoma cells. Brain Res Bull. 2010; 81(4–5): 428–433. [PubMed: 19932157]

24. Suzuki T, Tsukamoto I. Manganese-induced apoptosis in hepatocytes after partial hepatectomy. Eur J Pharmacol. 2005; 525(3):48–53. [PubMed: 16293243]

25. Tang C, Lee A, Volkmer J. Antibody against SSEA-5 glycan on human pluripotent stem cells enables removal of teratoma-forming cells. Nature Biotech. 2011; 29:829–834.

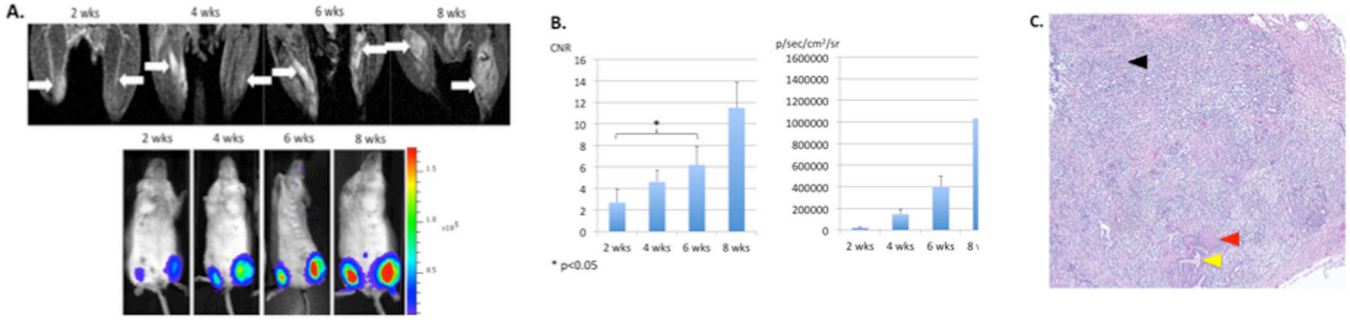

Figure 1. Longitudinal assessment of hESCs by MEMRI and BLI

A. Longitudinal MEMRI and BLI of SCID hind limbs. hESCs were indicated by white arrows in MEMRI. BLI of the corresponding mice showed gradually increased luciferase activity. **B** CNR of hESCs increased with cell proliferation and teratoma formation (left). Luciferase activity increased significantly with cell proliferatration at each time point (right). **C.** H & E staining showed teratoma formation at week 6. Endoderm was indicated by a yellow arrow, mesoderm by a red arrow, and ectoderm by a black arrow.

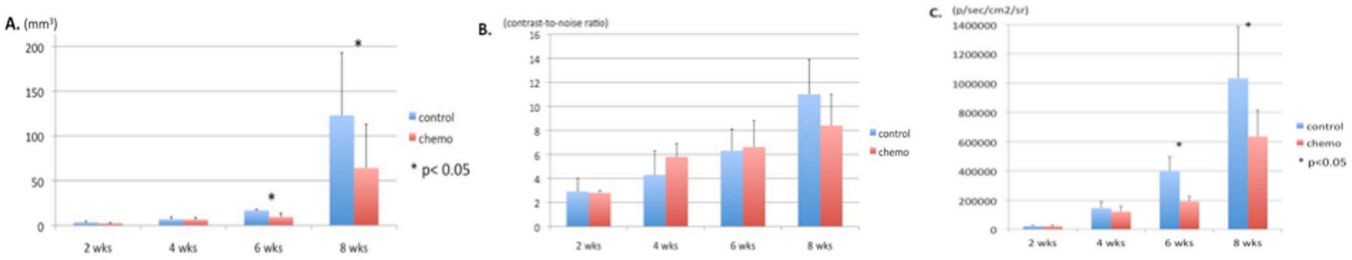

Figure 2. Longitudinal assessment of chemotherapy on the hESC derived teratoma

A. 3D volume obtained from MEMRI showed significant reduction in chemotherapy group compared with the control group in weeks 6 and 8 ($p<0.05$). **B.** Comparable CNR is noted between the chemotherapy and the control groups ($p>0.05$). There is a trend towards higher CNR in the chemotherapy than the control group at weeks 4 and 6, suggesting Mn^{2+} accumulation. This is followed by a trend towards lower CNR in the chemotherapy group at week 8, implying cell death and loss of intracellular Mn^{2+} ($p>0.05$). **C.** Average luciferase activity is significantly reduced in the chemotherapy group compared with the control group in weeks 6 and 8 ($p<0.05$).

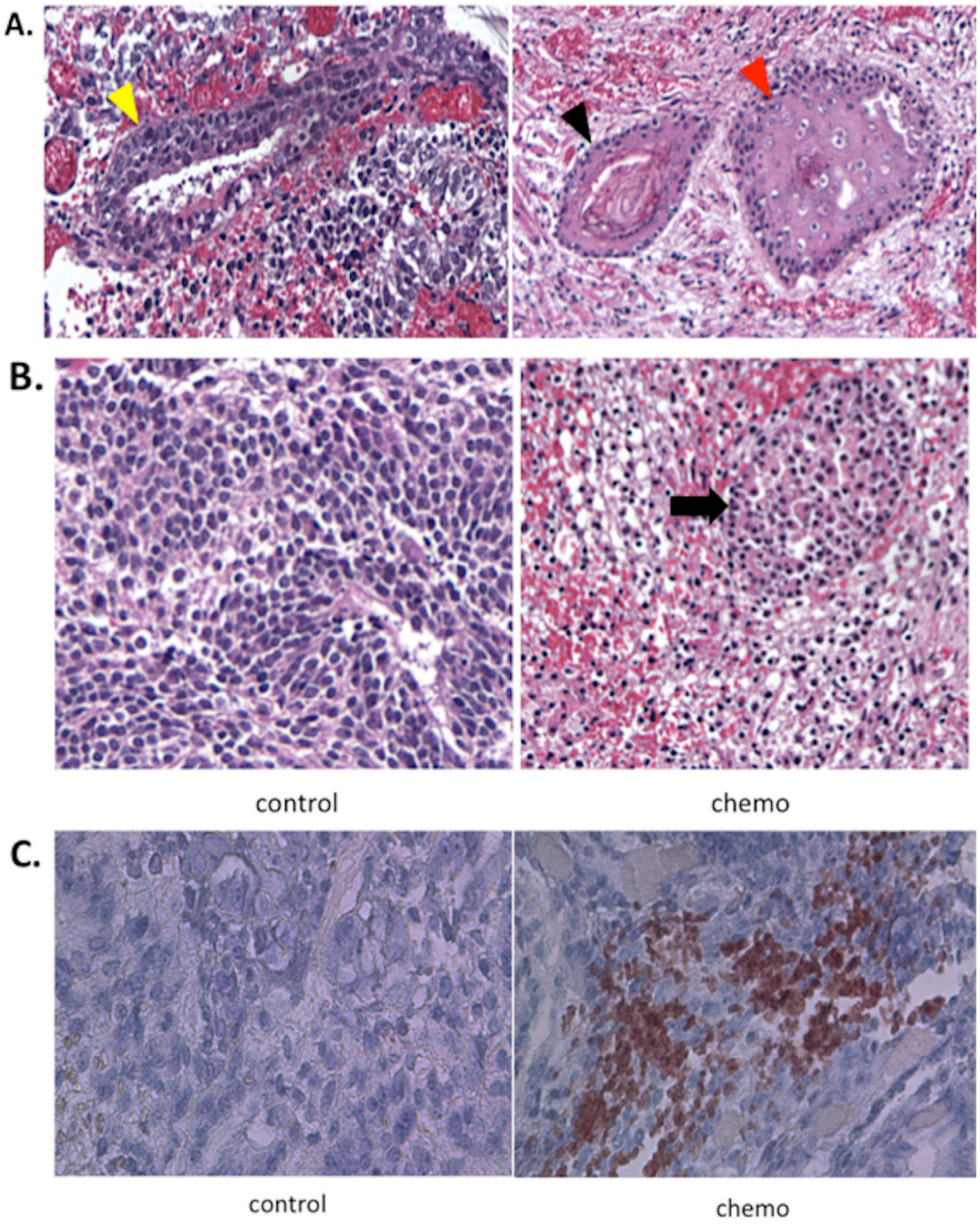

Figure 3. Teratoma formation and reduction

A. H&E staining shows both chemotherapy and control groups formed teratoma consisting of three different germ layers: endoderm (yellow arrow), ectoderm (black arrow) and mesoderm (red arrow). **B.** H&E staining of the chemotherapy group shows increased dead cells characterized by nuclear atypia and pyknosis shown as dark and small nuclei (indicated by a black arrow) with multiple focal hemorrhages. The control group does show only viable teratoma cells. **C.** Immunohistochemistry was positive for diffuse Caspase 3 (Brown color) signals from the treatment group, indicating apoptosis.